

## Detection of inter-hemispheric asymmetries of brain perfusion in SPECT

**B Aubert-Broche<sup>1</sup>, C Grova<sup>1</sup>, P Jannin<sup>1</sup>, I Buvat<sup>2</sup>, H Benali<sup>2</sup>  
and B Gibaud<sup>1</sup>**

<sup>1</sup> Laboratoire IDM, Faculté de Médecine, Université de Rennes 1, Rennes, France

<sup>2</sup> INSERM U494, CHU Pitié Salpêtrière, Paris, France

E-mail: berengere.broche@univ-rennes1.fr

Received 30 January 2003, in final form 26 March 2003

Published 20 May 2003

Online at [stacks.iop.org/PMB/48/1505](http://stacks.iop.org/PMB/48/1505)

### Abstract

Technetium-99m HMPAO and technetium-99m ECD single photon emission computed tomography (SPECT) imaging is commonly used to highlight brain regions with altered perfusion. It is particularly useful in the investigation of intractable partial epilepsy. However, SPECT suffers from poor spatial resolution that makes interpretation difficult. In this context, we propose an unsupervised voxel neighbourhood based method to assist the detection of significant functional inter-hemispheric asymmetries in brain SPECT, using anatomical information from MRI. For each MRI voxel, the anatomically homologous voxel in the contralateral hemisphere is identified. Both homologous voxel coordinates are then mapped into the SPECT volume using SPECT-MRI registration. Neighbourhoods are then defined around each SPECT voxel and compared to obtain a volume of inter-hemispheric differences. A volume including only the statistically significant inter-hemispheric differences is deduced from this volume using a non-parametric approach. The method was validated using realistic analytical simulated SPECT data including known asymmetries (in size and amplitude) as ground truth (gold standard). Detection performance was assessed using an ROC (receiver operating characteristic) approach based on the measures of the overlap between known and detected asymmetries. Validation with computer-simulated data demonstrates the ability to detect asymmetric zones with relatively small extension and amplitude. The registration of these detected functional asymmetries on the MRI enables good anatomical localization to be achieved.

(Some figures in this article are in colour only in the electronic version)

## 1. Introduction

Cerebral blood flow imaging is an essential tool in the investigation of intractable partial epilepsy. SPECT imaging is useful for detecting perfusion abnormalities, such as hyperperfusion in ictal SPECT and hypoperfusion in interictal SPECT, and helps localize the epileptogenic focus (Devous *et al* 1998).

Although in clinical routine the analysis of brain SPECT images is often limited to qualitative side-by-side visual inspection of the data, recent research has attempted to propose quantitative approaches. However, because the relationship between blood flow and  $^{99m}\text{Tc}$  HMPAO or  $^{99m}\text{Tc}$  ECD SPECT brain uptake is non-linear due to a saturation phenomenon, absolute measurement of regional cerebral blood flow (rCBF) from HMPAO/ECD SPECT scans is not feasible (Patterson and Wyper 1997). Therefore, only relative quantification methods have been proposed: region of interest (ROI) or volume of interest (VOI) based methods (Baird *et al* 1999, Kuji *et al* 1999, Migneco *et al* 1994) or voxel based methods studying either inter-scan and intra-subject variability (Zubal *et al* 1995, O'Brien *et al* 1998, Véra *et al* 1999) or inter-scan and inter-subject variability (Acton and Friston 1998, Lee *et al* 2000).

In this paper, we propose an unsupervised voxel neighbourhood based method for detecting inter-hemispheric asymmetries of brain perfusion in SPECT. In comparison with typical ROI or VOI based methods, our method avoids the problem of anatomical region delineation (Kang *et al* 2001). We consider our method to be complementary to voxel based methods that are mostly relevant in studies aiming at highlighting commonalities and differences either among different datasets of the same subject (Zubal *et al* 1995, O'Brien *et al* 1998, Véra *et al* 1999) or within a population of subjects (Van Bogaert *et al* 2000, Lee *et al* 2000).

First, we describe the proposed method for detecting inter-hemispheric asymmetries. Second, we present a validation using realistic simulated SPECT as gold standard and ROC analysis to determine the detection performance.

## 2. Material and methods

The proposed method aims at detecting inter-hemispheric functional asymmetries in brain SPECT images, using anatomical information available from magnetic resonance images (MRI). For this purpose, an asymmetry map is computed at the MRI spatial resolution. For each MRI voxel, the anatomically homologous voxel in the contralateral hemisphere is identified. Both homologous voxel coordinates are then mapped into the SPECT volume using SPECT-MRI registration. Neighbourhoods are then defined around each SPECT voxel and compared. A relative difference value is thus computed from both neighbourhoods and assigned to the MRI voxel to obtain a volume of inter-hemispheric differences (IHD volume). We then test the null hypothesis of this inter-hemispheric difference using a non-parametric approach. From this IHD volume and for a specific statistical threshold, a volume including only the statistically significant inter-hemispheric differences is deduced, designated as SSIHD volume.

The following sections describe the SPECT-MRI registration, the identification of homologous voxels and the creation of the IHD and SSIHD volumes. We then present the method used to validate the approach using simulated data.

### 2.1. Detection of inter-hemispheric functional asymmetries

*2.1.1. SPECT-MRI registration.* Approaches based on the optimization of statistical similarity measurements have proved to achieve accurate SPECT/MRI registration

(Barnden *et al* 2000). Using realistic simulations of normal and ictal SPECT, we compared main methods used for SPECT/MRI registration, namely mutual information (Maes *et al* 1997), normalized mutual information (Studholme *et al* 1999), correlation ratio (Roche *et al* 1998) and Woods' criterion (Woods *et al* 1993). Except for Woods' criterion, we found similar accuracy for these methods (Grova *et al* 2002). We thus chose to perform rigid SPECT/MRI registration using maximization of mutual information as described by Maes *et al* (1997).

*2.1.2. Identification of homologous regions.* For every voxel of the MRI volume, two approaches were proposed to determine the voxel which was anatomically homologous in the contralateral hemisphere. The first addresses situations in which the inter-hemispheric fissure can be considered as a plane and the eventual morphological asymmetry is limited to a difference in size in the medio-lateral direction. The second addresses more complex morphological asymmetries.

The first approach (Mip) consisted in manually defining the inter-hemispheric fissure used as symmetry plane on an MRI, as well as the boundaries of the hemispheres, to take into account any difference in size between the two hemispheres, based on the Talairach proportional squaring referential system (Talairach and Tournoux 1988).

The second approach (Msn) used the spatial normalization scheme provided in the Statistical Parametric Mapping (SPM) software package (Friston *et al* 1995). This method was used to compute a non-linear transformation between the MRI scan of the patient and the SPM T1 template which had been modified in order to be symmetrical. Using this transformation, the voxel corresponding to each point of the patient's MRI was identified in the template. Since the template is symmetric in its construction, the homologous voxel in the contralateral hemisphere was obtained by symmetry. By using the inverse deformation fields, the coordinates of the homologous voxel in the patient's MRI were determined. The voxel coordinates were then transferred to the SPECT volume to define voxel neighbourhoods.

*2.1.3. Creation of an inter-hemispheric difference (IHD) volume.* Two symmetrical spherical voxel neighbourhoods (diameter of 18 mm) containing 33 voxels were defined on SPECT data. The empirical means ( $\bar{x}_1$  and  $\bar{x}_2$ ) and the respective standard deviations ( $\sigma_1$  and  $\sigma_2$ ) of the voxel SPECT intensity values in both neighbourhoods were calculated and the normalized difference  $D$  defined by  $D = \frac{\bar{x}_1 - \bar{x}_2}{\sqrt{\sigma_1^2 + \sigma_2^2}}$  was deduced.

This result was stored in a volume of differences at the same coordinates as the initial voxel within the MR volume. The calculation was repeated for each MRI voxel in a brain mask to fill the IHD volume.

*2.1.4. Creation of the statistically significant inter-hemispheric differences (SSIHD) volume.* A volume was created by testing the hypothesis  $H_0: D = 0$  against  $H_1: D \neq 0$  at each MRI voxel and by assigning the associated p-value to the corresponding voxel of the volume. To perform the test, we proposed a non-parametric approach using the empirical estimation of the distribution of  $D$  under the null hypothesis  $H_0$ .

Voxel values of the difference volume were strongly correlated because of the poor spatial resolution of the SPECT images and of the use of overlapping adjacent voxel neighbourhoods. An empirical estimation of the distribution of  $D$  under the null hypothesis  $H_0$  was therefore obtained by selecting a set of uncorrelated voxels from the difference volume. From a study of the correlation between neighbour IHD voxels in the three directions of space (cf figure 1), it was found that samples located at a distance of at least 18 mm showed coefficients of correlation (CC) < 0.2. The coefficients of correlation were computed as

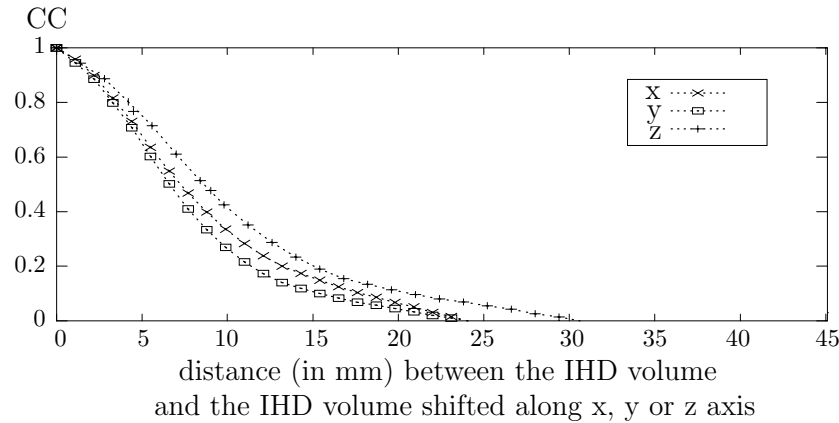


**Figure 1.** Correlation between neighbour IHD voxels in the three directions of space.

$$CC(\mathbf{d}, n) = \frac{\sum_{\mathbf{x}_k \in \Omega} (v(\mathbf{x}_k) - \bar{v})(v_s(\mathbf{x}_k) - \bar{v}_s)}{[\sum_{\mathbf{x}_k \in \Omega} (v(\mathbf{x}_k) - \bar{v})^2 \sum_{\mathbf{x}_k \in \Omega} (v_s(\mathbf{x}_k) - \bar{v}_s)^2]^{1/2}} \quad (1)$$

where  $\Omega$  is the voxel grid of the overlap between the brain mask on the IHD volume and the brain mask on the IHD volume shifted along  $n$  voxels in the direction  $\mathbf{d}$  (along  $x$ -,  $y$ - or  $z$ -axis),  $\mathbf{x}_k$  are voxels belonging to  $\Omega$ ,  $v(\mathbf{x}_k)$  is the value of the voxel  $\mathbf{x}_k$  in the IHD volume,  $v_s(\mathbf{x}_k) = v(\mathbf{x}_k + n\mathbf{d})$  is the value of the corresponding voxel  $\mathbf{x}_k$  in the IHD volume shifted along  $n$  voxels (voxel size = 1.1 mm  $\times$  1.1 mm  $\times$  1.1 mm) in the direction  $\mathbf{d}$  (along  $x$ -,  $y$ - or  $z$ -axis),  $\bar{v} = \frac{1}{\text{Card}(\Omega)} \sum_{\mathbf{x}_k \in \Omega} v(\mathbf{x}_k)$  and  $\bar{v}_s = \frac{1}{\text{Card}(\Omega)} \sum_{\mathbf{x}_k \in \Omega} v_s(\mathbf{x}_k)$ .

Since the distribution of  $D$  had to be established under the null hypothesis, outlier voxels located in asymmetric areas should be removed. These outliers should be few in number, assuming that the size of the asymmetrical areas is small with respect to the total volume of the brain. Voxels below the 1% quantile and above the 99% quantile of the distribution  $D$  were therefore removed. We thus obtained  $N$  uncorrelated samples ( $N \approx 130$ )  $D_{i,1 \leq i \leq N}$  to assess the distribution of  $D$  under  $H_0$ .

Selecting these  $N$  spatially uncorrelated voxels, the  $p$ -value associated with an observed  $D^*$  value at each voxel in the IHD volume was estimated as below,

$$p\text{-value}(D^*) = \frac{\#|D_i \geq D^*|}{N} \quad (2)$$

where  $\#|D_i \geq D^*|$  means the number of  $D_{i,1 \leq i \leq N}$  greater than  $D^*$ .

The  $p$ -value volume could then be thresholded to get a SSIHD volume highlighting only those voxels for which the null hypothesis was rejected at a given confidence level.

An illustrative example is provided in figure 2. It shows the MRI of an epileptic patient, the ictal SPECT registered on MRI, the IHD volume obtained with the Msn approach and a SSIHD volume corresponding to a threshold of 0.1%. The cross on the images is located on the epileptic focus.

## 2.2. Validation method

To determine the ability of our method to detect functional asymmetry zones of various sizes and amplitudes, in both anatomically symmetric and asymmetric brains, realistic SPECT datasets including known functional asymmetries (in size and amplitude) were simulated.

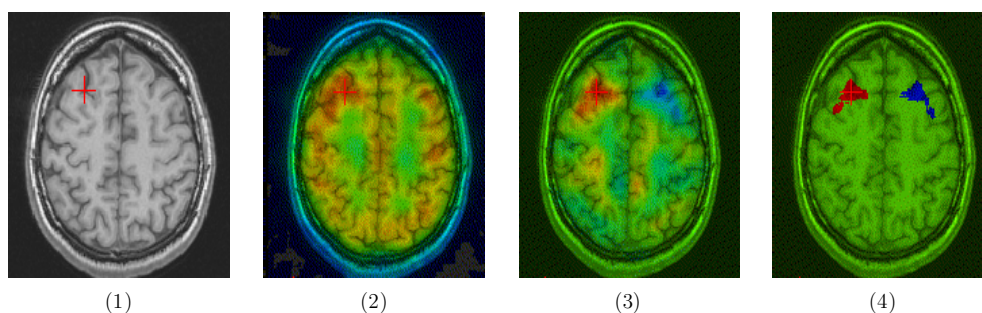


**Figure 2.** (1) MRI scan of an epileptic patient, (2) ictal scan registered on MRI (3) IHD volume (4) SSIHD volume (threshold: 0.1%).

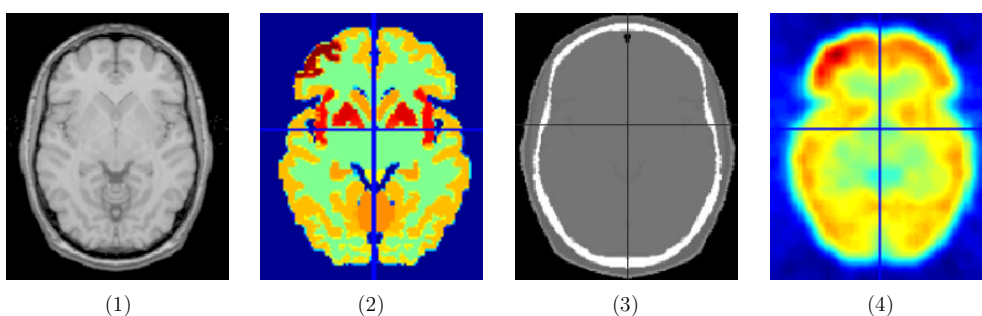


**Figure 3.** (1) Symmetric MR scan, (2) activity volume with a 10.3 cm<sup>3</sup> frontal asymmetric zone with amplitude values of +40% (3) attenuation volume (4) simulated SPECT.

Detection performance was assessed using an approach derived from the receiver operating characteristic (ROC) analysis (Metz 1986). ROC analysis was selected because it is known as a valuable tool to assess detection performance. Moreover, the conditions of application of ROC analysis are fulfilled: our simulation framework provides the ground truth and our detection method involves the choice of a decision threshold, needed to build ROC curves.

**2.2.1. SPECT simulations.** Realistic analytical SPECT simulations were performed using activity and attenuation maps defined from anatomical data (cf figure 3). These anatomical data were provided by the Zubal head phantom, consisting of 63 anatomical entities manually segmented and labelled from a normal T1-weighted MRI dataset (Zubal *et al* 1994). The attenuation map was derived from this segmented volume by associating a specific medium with each of the 63 entities, chosen among 8 attenuation media (conjunctive tissue, air, water, brain, bone, muscle, fat and blood). To construct the theoretical activity map, a theoretical model of brain perfusion, mimicking a mean normal perfusion, was established from real SPECT data (27 healthy subjects) as presented in (Grova *et al* 2001). To do so, these SPECT data were spatially transformed into a mean anatomy referential and quantitative measurements were made using the anatomical entity masks extracted from the labelled MRI, after spatial normalization.

These attenuation and activity maps were used to simulate SPECT projections taking into account non-uniform attenuation (64 projections  $128 \times 128$  over  $360^\circ$ , RecLBL software package (Huesman *et al* 1977)). Collimator and detector response were simulated using an 8 mm full width at half maximum (FWHM) Gaussian filter. Poisson noise was also

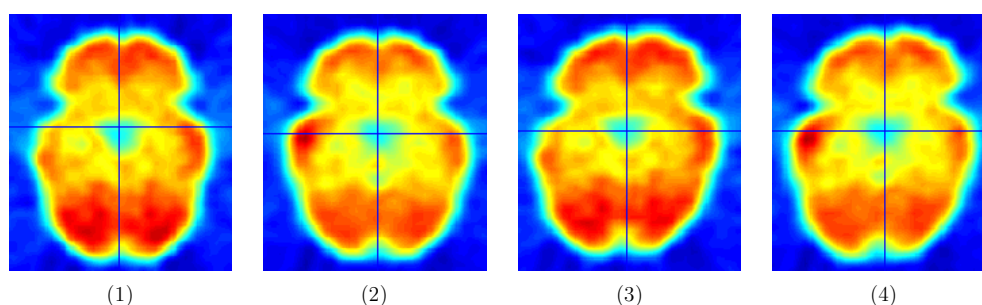


**Figure 4.** Simulated SPECT with a  $10.63 \text{ cm}^3$  temporal asymmetric perfusion abnormality corresponding to a 30% increased uptake (1), (3) and 30% decreased uptake (2), (4). Simulations (1) and (2) were based on a morphological symmetric brain, simulations (3) and (4) were based on a morphological asymmetric brain.

**Table 1.** Volume of the asymmetric zones simulated in the grey matter.

Size	Sphere radius	Frontal lobe	Occipital lobe	Parietal lobe	Temporal lobe
S1	5 mm	$0.88 \text{ cm}^3$	$0.91 \text{ cm}^3$	$1.19 \text{ cm}^3$	$1.15 \text{ cm}^3$
S2	10 mm	$2.67 \text{ cm}^3$	$2.55 \text{ cm}^3$	$2.81 \text{ cm}^3$	$2.88 \text{ cm}^3$
S3	15 mm	$5.50 \text{ cm}^3$	$4.76 \text{ cm}^3$	$5.30 \text{ cm}^3$	$5.76 \text{ cm}^3$
S4	20 mm	$10.30 \text{ cm}^3$	$9.36 \text{ cm}^3$	$11.14 \text{ cm}^3$	$10.63 \text{ cm}^3$

included on these projections. Images were reconstructed using filtered back-projection with a Nyquist frequency cutoff ramp filter and the reconstructed images were post-filtered using a 3D Gaussian filter with FWHM of 8.8 mm, leading to a resolution of 12 mm.

**2.2.2. Simulation of functional asymmetries.** We first simulated SPECT volumes without any anatomical asymmetry. We then introduced functional asymmetric zones of various sizes and intensities in the grey matter of the frontal, occipital, parietal or temporal lobes. The asymmetric zones were spheres with a radius of 5, 10, 15 or 20 mm, defined on the activity map. To model realistic perfusion abnormalities, only grey matter voxel values were increased or decreased (baseline activity plus or minus 10%, 20%, 30% or 40%). One hundred and twenty-eight different cases of functional asymmetries were introduced into the anatomically symmetric brain: combination of four localizations, four sizes (cf table 1) and eight amplitude values.

To assess the ability of the method to detect asymmetric functional zones within an anatomically asymmetric brain, anatomical asymmetry was introduced in our anatomical data. This was achieved by non-linear registration (Friston *et al* 1995) of the Zubal MRI scan with a patient MRI scan showing obvious anatomical asymmetry of brain hemispheres, the computed transformation was then used to deform our anatomical data. One hundred and twenty-eight different simulations were also computed from the anatomically asymmetric brain.

Figure 4 presents four examples of simulated SPECT images. The temporal asymmetric zone extension was  $10.63 \text{ cm}^3$  in all volumes and the perfusion abnormalities corresponded to a 30% increased and 30% decreased uptake. These simulations were based on a morphological symmetric and asymmetric brain.

**2.2.3. Overlap measurements.** Given the estimated asymmetry maps (IHD and SSIHD volumes), a degree of overlap between the actual asymmetric zone and the estimated one

(at a given statistical threshold) was calculated, by assigning voxels to true positives (TP), true negatives (TN), false positives (FP) and false negatives (FN). True positives were voxels belonging to both the significant zone in the statistical volume and to the actual asymmetric zone. The true negatives were voxels belonging to none of these two zones. The false positives were voxels belonging to the significant zone but not to the actual asymmetric zone. The false negatives were voxels belonging to the actual asymmetric zone but not to the significant one. Sensitivity ( $\frac{TP}{TP+FN}$ ) and specificity ( $\frac{TN}{TN+FP}$ ) were computed. Then, receiver operating characteristic curves (or ROC curves) (Metz 1986) were deduced by plotting the true positive rate (or sensitivity) against the false positive rate ( $1 - \text{specificity}$ ) for different statistical threshold values. The area under the ROC curve (AUC) was used as an index characterizing the detection performance of the method. The Wilcoxon rank sum test was used to test difference in performance between methods or between various parameters in the simulations.

Our method was applied to the 256 simulated SPECT volumes to detect simulated functional asymmetries in both morphologically symmetric and asymmetric brains. As we tested the two possible approaches to calculate anatomical homologous regions (Mip approach using inter-hemispheric plane and Msn using spatial normalization), we obtained 512 ROC curves and AUC values.

To test the influence of voxel neighbourhoods, we also applied the method with different sizes of voxel neighbourhoods (0.9, 1.8, 2.7 and 3.8 cm of diameter) for some simulated SPECT. The Wilcoxon rank sum test was used to test difference in performance according to the size used.

*2.2.4. Diagnostic impact.* In order to quantify the diagnostic impact of the method when reading SPECT images, we performed a localization ROC (LROC) analysis (Starr *et al* 1975). We asked two clinicians to analyse 20 SPECT simulations either with or without a functional asymmetry and to answer whether the image actually shows an abnormality using a certainty scale from 1 to 5, defined as 1: definitely no, 2: probably no, 3: possibly yes, 4: probably yes and 5: definitely yes. In addition, readers indicated the asymmetry localization. The reading was done either with or without the help of the IHD volume. Then, two LROC curves were deduced (with or without the help of the IHD volume) and compared.

### 3. Results

Figures 5 and 6 show some examples of ROC curves obtained with Mip (figure 5) and Msn (figure 6) approaches, applied to SPECT volumes simulated from an anatomically symmetric MRI with a  $10.3 \text{ cm}^3$  temporal asymmetry with different amplitude values.

AUC measurements (mean and standard deviation on the four anatomical localizations) are presented in table 2 for the two approaches (Mip versus Msn homologous regions computation) and for asymmetries simulated from a symmetric and an asymmetric anatomical MRI. Distributions of AUC measurements are also displayed using box-plot representations (cf figure 7).

As expected, the larger and the more intense the asymmetric zone, the more efficient the detection. Within a morphological symmetric brain, detection performances using the Mip approach were not significantly better than those using the Msn approach ( $p > 0.05$ , Wilcoxon test). However, for an asymmetric brain, detection performances using the Msn approach were significantly better than those using the Mip approach ( $p < 0.001$ , Wilcoxon test). Furthermore, for both symmetric and asymmetric brain, hypoperfusions were significantly

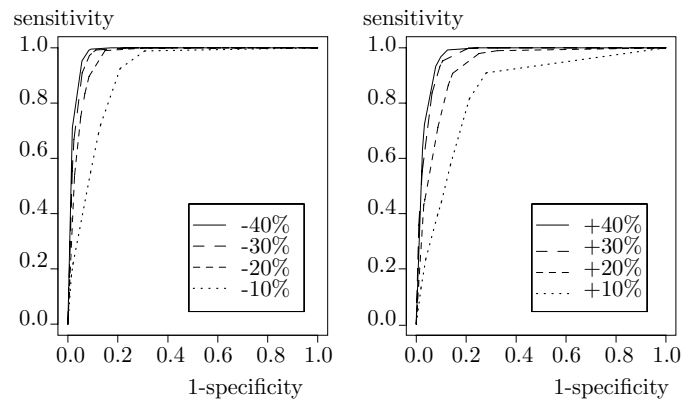


**Figure 5.** ROC curves for a temporal asymmetry of  $10.3 \text{ cm}^3$  with hypo (left) and hyperperfusion (right) simulated from a symmetric MRI (homologous regions calculated using the Mip approach).

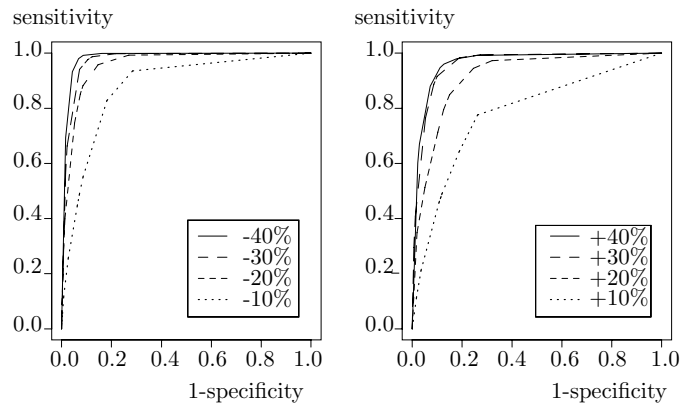


**Figure 6.** ROC curves for a temporal asymmetry of  $10.3 \text{ cm}^3$  with hypo (left) and hyperperfusion (right) simulated from a symmetric MRI (homologous regions calculated using the Msn approach).

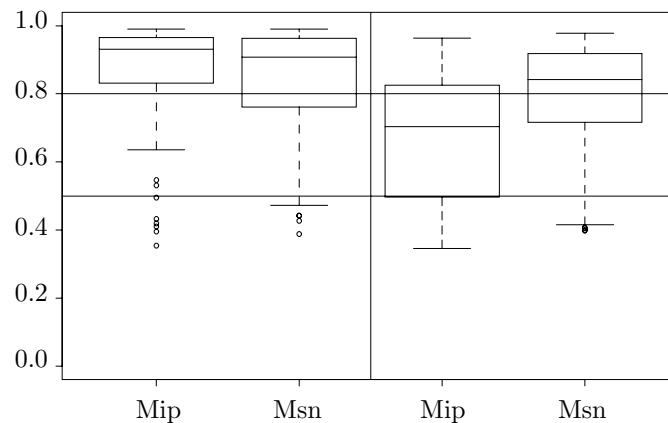


**Figure 7.** AUC distribution using box-plot representation for Mip and Msn approaches for asymmetries simulated from a symmetric (left) and asymmetric (right) anatomical MRI.

**Table 2.** Averaged AUC for functional asymmetries simulated from a symmetric (top) and asymmetric (bottom) anatomical MRI. Bold-faced values are greater than 0.8.

		Activity							
Size		+40%	+30%	+20%	+10%	-10%	-20%	-30%	-40%
Symmetric anatomical MRI									
Mip	S4	<b>0.97</b> (0.01)	<b>0.96</b> (0.02)	<b>0.93</b> (0.03)	<b>0.83</b> (0.05)	<b>0.86</b> (0.04)	<b>0.94</b> (0.03)	<b>0.97</b> (0.01)	<b>0.98</b> (0.01)
	S3	<b>0.96</b> (0.02)	<b>0.94</b> (0.02)	<b>0.93</b> (0.05)	0.79(0.10)	<b>0.83</b> (0.09)	<b>0.94</b> (0.03)	<b>0.97</b> (0.02)	<b>0.97</b> (0.01)
	S2	<b>0.94</b> (0.04)	<b>0.94</b> (0.04)	<b>0.88</b> (0.04)	0.77(0.08)	0.69(0.17)	<b>0.89</b> (0.08)	<b>0.93</b> (0.06)	<b>0.97</b> (0.02)
	S1	<b>0.93</b> (0.06)	<b>0.87</b> (0.07)	0.71(0.23)	0.57(0.27)	0.54(0.20)	0.80(0.12)	<b>0.87</b> (0.12)	<b>0.90</b> (0.13)
Msn	S4	<b>0.96</b> (0.01)	<b>0.94</b> (0.02)	<b>0.89</b> (0.03)	0.73(0.07)	<b>0.84</b> (0.05)	<b>0.94</b> (0.03)	<b>0.97</b> (0.01)	<b>0.98</b> (0.01)
	S3	<b>0.95</b> (0.03)	<b>0.92</b> (0.04)	<b>0.87</b> (0.09)	0.68(0.12)	<b>0.82</b> (0.08)	<b>0.93</b> (0.04)	<b>0.97</b> (0.02)	<b>0.98</b> (0.01)
	S2	<b>0.92</b> (0.07)	<b>0.90</b> (0.07)	0.80(0.09)	0.65(0.15)	0.70(0.13)	<b>0.88</b> (0.09)	<b>0.93</b> (0.05)	<b>0.96</b> (0.03)
	S1	<b>0.84</b> (0.14)	0.78(0.16)	0.63(0.23)	0.55(0.25)	0.60(0.12)	0.77(0.13)	<b>0.87</b> (0.12)	<b>0.90</b> (0.12)
Asymmetric anatomical MRI									
Mip	S4	0.75(0.11)	0.71(0.12)	0.67(0.12)	0.61(0.13)	0.64(0.20)	0.69(0.23)	0.73(0.24)	0.76(0.25)
	S3	0.70(0.12)	0.67(0.15)	0.65(0.14)	0.57(0.16)	0.66(0.23)	0.70(0.25)	0.72(0.26)	0.74(0.27)
	S2	0.66(0.15)	0.63(0.14)	0.61(0.15)	0.54(0.15)	0.66(0.24)	0.70(0.26)	0.72(0.27)	0.74(0.28)
	S1	0.58(0.21)	0.58(0.17)	0.53(0.15)	0.54(0.16)	0.65(0.25)	0.68(0.24)	0.71(0.25)	0.71(0.26)
Msn	S4	<b>0.93</b> (0.02)	<b>0.90</b> (0.04)	<b>0.85</b> (0.06)	0.70(0.07)	0.79(0.07)	<b>0.88</b> (0.09)	<b>0.94</b> (0.03)	<b>0.95</b> (0.03)
	S3	<b>0.91</b> (0.05)	<b>0.87</b> (0.06)	<b>0.82</b> (0.10)	0.65(0.12)	0.76(0.14)	<b>0.87</b> (0.09)	<b>0.92</b> (0.05)	<b>0.94</b> (0.04)
	S2	<b>0.88</b> (0.06)	<b>0.84</b> (0.09)	0.75(0.11)	0.63(0.11)	0.66(0.19)	<b>0.80</b> (0.02)	<b>0.86</b> (0.13)	<b>0.92</b> (0.06)
	S1	0.79(0.14)	0.71(0.16)	0.61(0.17)	0.54(0.20)	0.54(0.16)	0.63(0.21)	0.78(0.23)	<b>0.86</b> (0.10)

better detected than hyperperfusions ( $p < 0.001$ , Wilcoxon test). For S3 and S4 asymmetry sizes, the larger the voxel neighbourhoods, the more efficient the detection ( $p < 0.05$ , Wilcoxon test). It was not the case for S1 and S2 asymmetry sizes.

Figure 8 shows LROC curves obtained by the clinicians with and without the help of the IHD volume. The AUC values are 0.48 and 0.57, respectively, without and with the help of an IHD volume.

#### 4. Discussion

We proposed an unsupervised voxel neighbourhood based method for detecting inter-hemispheric asymmetries. The method was applied to simulated SPECT volumes to detect simulated functional asymmetries. The detection performances for simulated SPECT volumes show that the proposed method is reliable and sensitive. The use of realistic SPECT simulations for this first validation step provides a good comprehension of the performances of this method. Detection performances depend both on the approach used to compute homologous regions and on the characteristics of the perfusion asymmetries. In the presence of morphological asymmetry, the performances using the Msn approach are better owing to the spatial normalization that corrects for the morphological asymmetry. This is not the case with the Mip approach because in the presence of such asymmetries, the inter-hemispheric fissure cannot be modelled by a plane. The performance of detection is probably very sensitive to the partial volume effect. As no correction was made in our simulated datasets, this may contribute to the difference of detection between hypo and hyperperfusion, as suggested by Van Laere *et al* (2002) in a hyperperfusion simulation study.

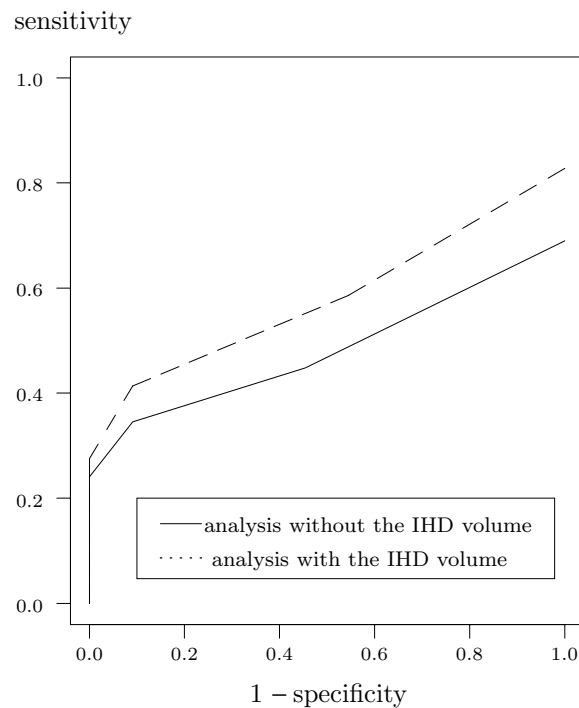


**Figure 8.** LROC curves obtained by the clinicians for the reading of SPECT simulations with or without the help of the IHD volume.

The detection performances may be influenced by some parameters of the method. The size of the spherical voxel neighbourhood used to compute difference volumes (diameter 1.8 cm, 33 voxels) was a trade-off: indeed it was large enough to take into account the spatial resolution of SPECT (12.2 mm) and to provide a sufficient number of measures, but not too large in order not to smooth and hide local differences. The effect of spatial normalization with regards to anatomical asymmetries should be further investigated. However, we may expect that it is not significant, since the same method proves very efficient to highlight activations in multi-subject fMRI studies (Ashburner and Friston 1997). The selection of the spatially uncorrelated voxels involved in the SSIHD volume computation could also influence the detection performances. The  $D$  distribution may actually vary, depending on the uncorrelated voxels that were selected. The impact of this variation on statistical volumes should be more precisely evaluated.

The proposed method primarily aims at highlighting slight perfusion asymmetries that can hardly be detected by visual inspection. In this respect, the results obtained in the study involving clinicians suggest an improvement of detection performance when the clinician has the IHD volume available.

To deduce the detection performances on SPECT data obtained in epileptic patients, the influence of SPECT-MRI registration should be studied. The simulations also did not simulate Compton scattering and depth-dependent collimator response that could also influence the detection performance.

The assumption used for the empirical estimation of the distribution of  $D$  that considered the asymmetric regions limited in size is consistent with the general aim of the method. In most

cases, sizes and amplitudes of asymmetries met in epilepsy are similar to those simulated and detected by our method. For large asymmetries as observed in some ictal SPECT cases, the method may not be relevant and needs to be adapted to enable the detection of slight secondary asymmetries hidden by primary hyperperfusion in the epileptogenic focus (for instance, slight secondary hyperperfusion in basal ganglia).

The method detects all significant functional asymmetries, which may be pathological or normal (Van Laere *et al* 2001). It should be interesting to determine whether a detected asymmetry is pathological or not, through comparisons with normal perfusion asymmetries measured from a control group (Van Bogaert *et al* 2000).

Alternatives to voxel neighbourhood based methods are ROI based or VOI based methods and voxel based methods. ROIs or VOIs may be geometric (Baird *et al* 1999) or may follow the boundaries of anatomical structures (Kuji *et al* 1999). They may be positioned manually or with the assistance of an anatomical atlas or template (Migneco *et al* 1994), or of the MRI of the patient (Julin *et al* 1997). In comparison with these approaches, the proposed method avoids the problem of delineating anatomical regions, which depends on the clinical context (Kang *et al* 2001).

Voxel based methods aim at studying either inter-scan and intra-subject variability (Zubal *et al* 1995, O'Brien *et al* 1998, Véra *et al* 1999) or inter-scan and inter-subject variability (Acton and Friston 1998, Signorini *et al* 1999, Lee *et al* 2000). In the detection of epileptogenic foci, a well-known intra-subject method consists in subtracting ictal and interictal SPECT, after they had been co-registered to MRI (Zubal *et al* 1995, O'Brien *et al* 1998, Véra *et al* 1999). Inter-subject approaches using Statistical Parametric Mapping (SPM) usually consist in a comparison between scans of an epileptic subject and a control group (Lee *et al* 2000). However, this last approach is considered as 'fairly conservative' (Acton and Friston 1998) due to smoothing, multiple comparisons correction and the limited number of scans usually involved. Unlike SPM approach, the proposed intra-scan method does not require any database of normal cases for the detection of inter-hemisphere asymmetries.

We believe that our approach of studying intra-scan and inter-hemisphere asymmetry is different and complementary. The relevance of studying the inter-hemispheric variations was confirmed in a PET study concerning the detection of hypometabolism in patients with temporo-mesial epilepsy (Van Bogaert *et al* 2000).

## 5. Conclusion

An unsupervised method for detecting functional inter-hemispheric asymmetry in SPECT images was described, based on the registration of SPECT images with corresponding MR images. One particularity lies in the fact that the method takes into account the eventual morphological asymmetries in the estimation of functional asymmetries, with two approaches addressing various degrees of morphological asymmetries. The originality of this approach consists in correcting any morphological asymmetries to detect the functional inter-hemispheric asymmetries. When the inter-hemispheric fissure is relatively planar, the correction consists in taking into account any difference in size between the hemispheres. When the inter-hemispheric fissure is not planar, spatial normalization is used to compute a non-linear transformation between the MRI and a symmetric template. Registration of the detected functional asymmetries on the MRI enables good anatomical localization to be achieved.

Validation with computer-simulated SPECT data demonstrates the ability to detect asymmetric zones with relatively small extension and amplitude. However, clinical validation in the context of epilepsy is required to complement this validation on simulated datasets.

## Acknowledgments

The authors wish to acknowledge Drs. Florence Prigent and Arnaud Biraben for their participation as readers in this study.

## References

- Acton P and Friston K 1998 Statistical parametric mapping in functional neuroimaging: beyond PET and fMRI activation studies *Eur. J. Nucl. Med.* **25** 663–7
- Ashburner J and Friston K 1997 The role of registration and spatial normalization in detecting activations in functional imaging *Clinical MRI* **7** 26–8 (webpage <http://www.fil.ion.ucl.ac.uk/spm/dox.html>)
- Baird A, Donnan G, Austin M, Hennessy O, Royle J and McKay W 1999 Asymmetries of cerebral perfusion in a stroke-age population *J. Clin. Neurosci.* **6** 113–20
- Barnden L, Kwiatek R, Lau Y, Hutton B, Thurjfell L, Pile K and Rowe C 2000 Validation of fully automatic brain SPET to MR co-registration *Eur. J. Nucl. Med.* **27** 147–54
- Devous M, Thisted R, Morgan G, Leroy R and Rowe C 1998 SPECT brain imaging in epilepsy: a meta-analysis *J. Nucl. Med.* **39** 285–93
- Friston K, Ashburner J, Poline J, Frith C, Heather J and Frackowiak R 1995 Spatial registration and normalization of images *Hum. Brain. Mapp.* **2** 165–89
- Grova C, Biraben A, Scarabin J, Jannin P, Buvat I, Benali I and Gibaud B 2001 A methodology to validate MRI/SPECT registration methods using realistic SPECT simulated data *Lecture Notes in Computer Science (MICCAI01)* vol 2208 (Berlin: Springer) pp 275–82
- Grova C, Jannin P, Biraben A, Buvat I, Benali H, Bernard A, Scarabin J and Gibaud B 2002 Validation of MRI/SPECT similarity-based registration methods using realistic simulations of normal and pathological SPECT data *Computer Assisted Radiology and Surgery 2002, Paris* (Berlin: Springer) pp 450–5
- Huesman R, Gullberg G, Greenberg W and Budinger T 1977 RECLBL library users manual, Donner algorithms for reconstruction tomography *Technical-Report Pub 214*, Lawrence Berkeley Laboratory, University of California
- Julin P, Lindqvist J, Svensson L, Slomka P and Wahlund L 1997 MRI-guided SPECT measurements of medial temporal lobe blood flow in Alzheimer's disease *J. Nucl. Med.* **38** 914–9
- Kang K, Lee D, Cho J, Lee J, Yeo J, Lee S K, Chung J K and Lee M 2001 Quantification of F-18 FDG PET images in temporal lobe epilepsy patients using probabilistic brain atlas *Neuroimage* **14** 1–6
- Kuji I, Sumiya H, Niida Y, Takizawa N, Ikeda E, Tsuji S and Tonami N 1999 Age-related changes in the cerebral distribution of <sup>99m</sup>Tc-ECD from infancy to adulthood *J. Nucl. Med.* **40** 1818–23
- Lee J, Kim H, Lee B, Kim O, Jeon T and Kim M 2000 Evaluation of ictal brain SPET using statistical parametric mapping in temporal lobe epilepsy *Eur. J. Nucl. Med.* **27** 1658–65
- Maes F, Collignon A, Vandermeulen D, Marchal G and Suetens P 1997 Multimodality image registration by maximization of mutual information *IEEE Trans. Med. Imaging* **16** 187–98
- Metz C 1986 ROC methodology in radiologic imaging *Invest. Radiol.* **21** 720–32
- Migneco O, Darcourt J, Benoliel J, Martin F, Robert P, Bussiere-Lapalus F and Mena I 1994 Computerized localization of brain structures in single photon emission computed tomography using a proportional anatomical stereotaxic atlas *Comput. Med. Imaging Graph* **18** 413–22
- O'Brien T, O'Connor M, Mullan B and Brinkmann B 1998 Substraction ictal SPECT co-registered to MRI in partial epilepsy: description and technical validation of the method with phantom and patient studies *Nucl. Med. Commun.* **19** 31–45
- Patterson J and Wyper D 1997 *SPECT Imaging of the Brain* (Dordrecht: Kluwer) ch 1 pp 1–42
- Roche A, Malandain G, Pennec X and Ayache N 1998 The correlation ratio as a new similarity measure for multimodal image registration *Lecture Notes in Computer Science (MICCAI'98)* (Berlin: Springer) pp 1115–24
- Signorini M, Paulesu E, Friston K, Perani D, Colleluori A, Lucignani G, Grassi F, Bettinardi V, Frackowiak R and Fazio F 1999 Rapid assessment of regional cerebral metabolic abnormalities in single subjects with quantitative and non-quantitative 18F-FDG PET: a clinical validation of statistical parametric mapping *Neuroimage* **9** 63–80
- Starr S, Metz C, Lusted L and Goodenough D 1975 Visual detection and localization of radiographic images *Radiology* **116** 533–8
- Studholme C, Hill D and Hawkes D 1999 An overlap invariant entropy measure of 3D medical image alignment *Pattern Recognit.* **32** 71–86
- Talairach J and Tournoux P 1988 *Co-Planar Stereotaxic Atlas of the Human Brain* (New York: Thieme)
- Van Bogaert P, Massager N, Tugendhaft P, Wikler D, Damhaut P, Levivier M, Brotchi J and Goldman S 2000 Statistical parametric mapping of regional glucose metabolism in mesial temporal lobe epilepsy *Neuroimage* **12** 129–38

- Van Laere K, Versijpt J, Audenauert K, Koole M, Goethals I, Achten E and Dierckx R 2001  $^{99m}\text{Tc}$ -ECD brain perfusion SPET: variability, asymmetry and effect of age and gender in healthy adults *Eur. J. Nucl. Med.* **28** 83–887
- Van Laere K, Versijpt J, Koole M, Vandenberghe S, Lahorte P, Lemahieu I and Dierckx R 2002 Experimental performance assessment of SPM for SPECT neuroactivation studies using a subresolution sandwich phantom design *Neuroimage* **16** 200–16
- Véra P, Kaminska A, Cieuta C, Hollo A, Stievenart J, Gardin I, Ville D, Mangin J, Plouin P, Dulac O and Chiron C 1999 Use of subtraction ictal SPECT co-registered to MRI for optimizing the localization of seizure foci in children *J. Nucl. Med.* **40** 786–92
- Woods R P, Mazziotta J C and Cherry S R 1993 MRI-PET registration with automated algorithm *J. Comput. Assist. Tomogr.* **17** 536–46
- Zubal I, Harrell C, Smith E, Rattner Z, Gindi G and Hoffer P 1994 Computerized three-dimensional segmented human anatomy *Med. Phys.* **21** 299–302
- Zubal I, Spencer S, Iman K and Smith O 1995 Difference images calculated from ictal and interictal technetium-99m-HMPAO SPECT scans of epilepsy *J. Nucl. Med.* **36** 684–9